Analysis of some preliminary simulations of Keplerian turbulence

By Javier Jiménez†, S. C. Kassinos‡ AND A. A. Wray

We present simulations of rotating sheared turbulence both for the Keplerian case, $2\Omega/S = 4/3$, and for $2\Omega/S = -4/3$. Both cases are linearly stable, and all the simulations decay, but there is a strong effect of the Reynolds number that is clearly visible in the different long-term behaviors of the simulations in large and in small computational grids. While the latter enter an apparently viscous regime for $St = O(1)$, the former track the inviscid rapid distortion theory (RDT) solutions for much longer times. The RDT solutions in both cases decay with a similar power-law exponent, $-1/2$, but the Keplerian case undergoes an appreciable initial transient growth that is absent in the other case. There are indications of nonlinear growth in a range of wavenumbers that could lead to self-sustaining turbulence in protoplanetary accretion disks. This secondary peak is present for both shear ratios, and is associated in both cases with eddy Rossby numbers of the order of 10^{-2}, and with eddy Reynolds numbers larger than a few hundred. Although additional simulations are needed, the above observations suggest the range of parameters in which to search for self-sustaining Keplerian turbulence, and emphasize the importance of simulations with higher resolutions and Reynolds numbers than those that have been used in the study of this problem up to this point.

1. Introduction

A long-standing problem in astrophysics is that, while most of the mass of planetary systems resides in the central star, most of their angular momentum is in the planets. Since it is commonly accepted that planets condense from accretion disks that share their origin with the central star, the preceding observation implies that the angular momentum of the original interstellar cloud must have been redistributed outwards during the accretion process. An order-of-magnitude analysis of time scales shows that this can only be achieved if the accretion is turbulent. Molecular viscosity is too weak by a factor of at least 10^4 to dissipate the required energy in the observed accretion times. Recent reviews of this issue can be found in Papaloizou and Lin (1995), Stone *et al.* (2000), and Balbus (2003).

The simulation of a complete accretion disk is beyond the power of present computers. The simplest reduction is the limit of a small sheared box, which studies a gas parallelepiped in the vicinity of the midplane of the disk, in rotating axes advected with the orbital velocity of its center of gravity. The coordinates can be considered locally Cartesian if the box size is small with respect to the thickness of the disk. Compressibility can be neglected, and the only remaining gravitational effect is a radial shear that models the variation of the orbital velocity with the distance from the central star (Umurhan

† Also, School of Aeronautics, Universidad Politécnica, 28040 Madrid, Spain
‡ Mechanical and Manufacturing Engineering, University of Cyprus, 1678 Nicosia, Cyprus

and Regev 2004). The coordinates and the basic box deformation are defined in figure 1. The azimuthal, radial, and disk-normal directions are x_1, x_2, and x_3.

If the orbital velocity decreases with the radius as $r^{-\xi}$, the ratio between the orbital angular velocity Ω and the shear rate S is

$$\chi = 2\Omega/S = 2/(1+\xi). \tag{1.1}$$

In the Keplerian case in which the mass of the disk is negligible with respect to the central star, $\xi = 1/2$ and $\chi = 4/3$. In the astrophysical literature this parameter is some times expressed as $q = 2/\chi$, but the present definition is more common in turbulence modeling.

While the mean flow is defined uniquely by χ, the evolution of the fluctuations also depends on the Rossby number,

$$Ro = \frac{u}{SL}, \tag{1.2}$$

which is the ratio between the time scale S^{-1} of the shear, to that of the turbulent fluctuations, L/u, and on the Ekman number

$$\varepsilon = \frac{\nu}{SL^2}, \tag{1.3}$$

which is the inverse of a Reynolds number.

Note that both Ro and ε have been defined in terms of the shear rate instead of the angular velocity, but the difference is immaterial in the Keplerian case because of (1.1).

It turns out that a uniform flow satisfying (1.1) is linearly stable to small hydrodynamic perturbations, and that one of the central problems of disk evolution is therefore how turbulence is generated under such conditions. It was originally expected that, since the Reynolds numbers involved are high, the flow would eventually transition to turbulence even in the absence of suitable linear hydrodynamic instabilities (Dubrulle and Zahn 1991; Dubrulle 1993; Dubrulle *et al.* 2005). Note that the problem is not so much whether a laminar flow, which is probably not a reasonable initial condition in accretion, would spontaneous transition to turbulence, but whether an initially turbulent state would eventually laminarize. However, up to now, numerical simulations have failed to generate self-sustaining or growing Keplerian turbulence for any set of initial conditions (Balbus *et al.* 1996).

There are numerous alternatives to pure hydrodynamic processes to make disks unstable, generally involving magnetic fields or radiative heating. Besides the general review articles mentioned at the beginning of this introduction, Lin and Papaloizou (1996) survey the application to observed disks, and Calvet *et al.* (2000) examine the case for episodic accretion. Disks span a wide range of parameters, from hot thick ones around black holes, to thin, slowly evolving, and relatively cold ones around young stars. It is only the latter which are thought to be involved in planet formation, while most non-hydrodynamic instabilities apply only to cases which are hot enough for the gas to be ionized or convectively unstable. Only the thin cold case will be of interest here.

The basic equilibrium theory of viscous accretion disks (Lynden-Bell and Pringle 1974) is summarized in Pringle (1981). Their thickness is dictated by the equilibrium between the gas pressure and gravity, and is of the order of

$$H = c/\Omega, \tag{1.4}$$

where c is the speed of sound. In protoplanetary disks the planet-forming region lies between $0.5 - 30$ AU (1 AU $= 1.5 \times 10^{11}$ m), where the temperature is between 10 and

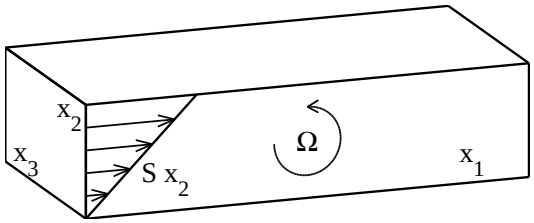

FIGURE 1. Definition of coordinates and positive sense of the basic deformation.

1000 °K. This implies disk aspect ratios of the order of 1:10, agreeing with observations. The eddy viscosity of the disk was first parameterized by Shakura and Sunyaev (1973) as

$$\nu_T = \alpha c H = \alpha c^2/\Omega, \tag{1.5}$$

where α is an empirical parameter. Hot disks around novae and black holes have accretion rates compatible with $\alpha = 0.1 - 1$, which can be explained in terms of the magnetic and thermal instabilities mentioned above. Protoplanetary disks have $\alpha = 10^{-3} - 10^{-2}$ (Beckwith and Sargent 1993; Lin and Papaloizou 1996), which is consistent with those disks being too cold to sustain the previously mentioned instabilities. This, however, leaves unanswered the question of how the required turbulence is generated.

Note that, if we assume that (1.4) gives the scale of the turbulent fluctuations, and that $\nu_T \approx u_T H$, the parameter α defined in (1.5) is essentially a Rossby number

$$\alpha = \frac{u_T H}{cH} \approx \frac{u_T}{\Omega H}. \tag{1.6}$$

This formula can also be used to estimate the intensity of the expected velocity fluctuations.

2. The rapid distortion limit

We express the flow in terms of a fluctuating velocity $\mathbf{u}$ with respect to the mean orbital rotation and shear, and let the frame of reference rotate with Ω. The equations of motion in the rotating frame, normalized with the shear rate and with some reference length L, are

$$\begin{aligned} [\partial_t + x_2\partial_1]\, u_1 + (1-\chi)u_2 - H_1 + \partial_1 p &= \varepsilon\nabla^2 u_1, \\ [\partial_t + x_2\partial_1]\, u_2 + \chi u_1 - H_2 + \partial_2 p &= \varepsilon\nabla^2 u_2, \\ [\partial_t + x_2\partial_1]\, u_3 - H_3 + \partial_3 p &= \varepsilon\nabla^2 u_3, \end{aligned} \tag{2.1}$$

where the $H_i = -u_j\partial_j u_i$ are the nonlinear advection terms.

The stability properties of the flow depend on the geometry of the mean flow in inertial axes, $\mathbf{u}_I = [(1-\chi/2)x_2,\, \chi x_1/2,\, 0]$. When $\chi < 0$ or $\chi > 2$, the inertial streamlines are elliptic, while the cases $0 < \chi < 2$ are hyperbolic. The special case $\chi = 1$ is an irrotational strain whose principal axes rotate in time, and $\chi = 0$ and $\chi = 2$ correspond to pure shears, with their mean velocities oriented respectively in the azimuthal and radial directions. They are not equivalent in the rotating frame of reference, because strain and rotation are not treated symmetrically.

When the gradients of the fluctuations are small with respect to S, or equivalently, when $Ro \ll 1$, the nonlinear terms in (2.1) can be neglected with respect to the shear

and to the rotation; the equations then become linear and homogeneous. In this "rapid distortion" limit, the solution of the initial value problem in an unbounded or periodic domain can be expressed as sums of elementary basis functions of the form

$$u_j = \widehat{u}_j(t) \exp\left[\mathrm{i} k_m(t) x_m\right]. \tag{2.2}$$

A recent survey of that limit can be found in Cambon and Scott (1999).

Nonuniform elliptic inviscid flows are subject to a linear parametric instability that survives at moderate Reynolds numbers (Pierrehumbert 1986). For uniform flows, stability depends on the sign of $B = \chi(1-\chi)$. When $B > 0$, in $0 < \chi < 1$, the flow is exponentially unstable (Bradshaw 1969; Pedley 1969). Since it follows from (1.1) that the orbital circulation decreases in this case with the distance from the star, this behavior is just a manifestation of Rayleigh's (1917) centrifugal instability. In the linear limit, the vortices in these flows are stretched and amplified along one of the characteristic directions, but their size also decreases, and viscosity eventually kills all perturbations. The Keplerian flow is in the stable hyperbolic range, $B < 0$, and is treated below in some detail.

We will initially consider the flow to be inviscid. When (2.2) is substituted in (2.1), the wavenumbers and amplitudes are found to satisfy

$$\begin{aligned} k_1 &= k_1(0) \equiv k_{10}, \\ k_2 &= k_{20} - k_{10} t, \\ k_3 &= k_{30}. \end{aligned} \tag{2.3}$$

and

$$\partial_t \widehat{\mathbf{u}} = \begin{pmatrix} \chi\gamma_1\gamma_2 - \varepsilon k^2 & \chi - 1 + (2-\chi)\gamma_1^2 & 0 \\ \chi(\gamma_2^2 - 1) & (2-\chi)\gamma_1\gamma_2 - \varepsilon k^2 & 0 \\ \chi\gamma_2\gamma_3 & (2-\chi)\gamma_1\gamma_3 & -\varepsilon k^2 \end{pmatrix} \widehat{\mathbf{u}}, \tag{2.4}$$

where $\gamma_j = k_j/k$, and $k^2 = k_j k_j$ is the squared wavenumber magnitude.

Salhi and Cambon (1997) give analytic solutions for the evolution of some flow quantities in the general case, in terms of hypergeometric functions, and Akylas *et al.* (2006) have done the same for the case $\chi = 1$, but it is usually only possible to give analytic results for some combinations of parameters. The behavior for long times is easier to obtain. If $k_{10} \neq 0$, the stream- and span-wise wavenumbers remain constant, but the magnitude of the radial wavenumber increases without bound as the flow is sheared. In the limit $k_{01} t \to \infty$ of very large deformations, $k_2 \to -k_{01} t$, γ_1 and γ_3 tend to zero, and $\gamma_2 \to -1$.

That limit gives little information about the eventual fate of the solution, except that $\widehat{u}_2$ has to decay faster than the other two components because of the incompressibility constraint. The more interesting question of the behavior of the solution for large finite times can be studied by assuming that

$$\widehat{u}_1 \approx b_1 t^\delta, \quad \widehat{u}_2 \approx b_2 t^{\delta-1}, \quad \widehat{u}_3 \approx b_3 t^\delta. \tag{2.5}$$

When this is substituted into the inviscid version of (2.4), keeping only the leading order for long times, we obtain an eigensystem for the b_j that only has non-trivial solutions if

$$\delta_\pm = -\frac{1}{2} \pm \frac{1}{2}(1 + 4\sigma_{30}^2 B)^{1/2}, \tag{2.6}$$

where $\sigma_{j0} = k_{j0}/k_{10}$ and B is the Bradshaw–Pedley stability parameter. If $B > 0$, one of the roots in (2.6) is positive, and perturbations grow exponentially. Otherwise, all the

roots are stable, and become oscillatory for σ_{30} large enough. The eigenvectors associated with those eigenvalues are

$$\mathbf{b}_\pm = [\chi - 1,\, \chi + \delta_\pm,\, -\delta_\mp/\sigma_{30}]\,. \tag{2.7}$$

There is a third eigenvalue, $\delta_3 = 0$, whose eigenvector is $\mathbf{b_3} = [0,\, 0,\, 1]$. It corresponds to arbitrary velocity perturbations normal to the orbital plane, which are unaffected by the orbital motion.

This eigensystem degenerates for several combinations of parameters, opening the possibility of more complex behaviors. The two cases with $B = 0$ do not directly concern us here, but they are useful for comparison. In both cases, linear theory predicts that most perturbations decay exponentially, but that infinitely long perturbations aligned to the mean flow, $k_{10} = 0$, grow algebraically (linearly) until they are eventually damped by viscosity. The amplification during this "transient growth" phase can be substantial, and, for sufficiently high Reynolds numbers, it creates structures that may grow until nonlinearity becomes important.

In the special case of pure shear in inertial axes, $\chi = 0$, the resulting nonlinear turbulence is thought to grow exponentially, both from numerical (Rogers and Moin 1987) and from experimental evidence (Tavoularis and Karnik 1989). The transient structures in this situation are long streaks of u_1, oriented along x_1, and the exponential growth is thought to be powered by their secondary instability.

In the case of a rotating strain, $\chi = 1$, the predicted linear growth is slower than in the inertial case. Nonlinear large-eddy simulations by Bardina (1983) give a growth rate that is even slower than the linear prediction, with no trace of exponential behavior. Direct simulations at higher resolution by Brethouwer (2005), although still growing only linearly, do so at a rate intermediate between the one predicted by RDT at the same Reynolds number, and the higher inviscid one predicted by Akylas *et al.* (2006). In this latter direct simulation, the shear stress parameter $\langle u_1 u_2\rangle/u'^2$ does not seem to be vanishing at the end of the simulation, suggesting that the growth might really be weakly exponential, but the simulation is too short to draw firm conclusions. The disagreement between the large-eddy and the direct simulations is probably due to the limited Reynolds numbers; the asymptotic high-Reynolds number behavior of turbulence in this case is unknown.

The two-dimensional Taylor–Proudman limit, $k_{30} = 0$, is of more immediate interest. In that case one of the eigenvectors in (2.7) is lost, the vertical vorticity ω_3 is invariant, and the solution to the full linearized equations (2.4) can be written in closed form as (Umurhan and Regev 2004),

$$\begin{aligned}
\widehat{u}_1 &= \mathrm{i}\,\widehat{\omega}_{30}\frac{k_2}{k^2} = \frac{\mathrm{i}\,\widehat{\omega}_{30}}{k_{10}}\,\frac{\sigma_{20} - t}{1 + (\sigma_{20} - t)^2}, \\
\widehat{u}_2 &= -\mathrm{i}\,\widehat{\omega}_{30}\frac{k_1}{k^2} = -\frac{\mathrm{i}\,\widehat{\omega}_{30}}{k_{10}}\,\frac{1}{1 + (\sigma_{20} - t)^2},
\end{aligned} \tag{2.8}$$

Note that these results are independent of χ, and that, even if both velocity components eventually decay, as $1/t$ and $1/t^2$ respectively, they can initially be substantially amplified. This happens to oblique perturbations that are initially tilted 'the wrong way', $\sigma_{20} > 0$. As the evolution in (2.3) shears k_2 through zero, before making it large and negative, k decreases, and both velocity components are amplified. In essence vortex sheets which are almost aligned to the flow, become compact vortices before being sheared again into sheets tilted in the opposite direction. It follows from (2.8) that the maximum

amplification of the modal energy is $1+\sigma_{20}^2$, and happens at $t=\sigma_{20}$. Note that the wavenumber k_2 does not increase during this initial phase, so that there is no reason for u_2 to decay faster than the other two components. In fact, u_2 is the most amplified component in (2.8).

The degeneracy in this case arises because δ_+ tends to zero, and its eigenvector aligns with $\mathbf{b_3}$. Significant transient growth is therefore likely to persist in nearly two-dimensional cases in which the angle between the two eigenvectors remains small, and one of the two eigenvalues in (2.6) is close to neutral (Schmid and Henningson 2001). Numerical experimentation suggests that very large amplifications are indeed a feature of all cases in which $\sigma_{20}\gg 1$.

Another eigenvalue collision occurs when $\sigma_{30}^2=-1/4B$, which marks the boundary between oscillatory and power-law long-term behavior of the solutions. In those cases $\delta_+=\delta_-=-1/2$ and their eigenvectors are also identical. Numerical experimentation suggests that one of the two eigensolutions picks a logarithmic factor, but that this is not enough to affect its stability properties.

The remaining case is $k_{10}=0$, in which the wave vector remains constant, and the large-deformation limit is never reached. These are the wave vectors that undergo maximum transient growth in the case of inertial shear. In the rotating case, (2.4) becomes

$$\partial_t \widehat{\mathbf{u}} = \begin{pmatrix} 0 & \chi-1 & 0 \\ -\chi\gamma_{30} & 0 & 0 \\ \chi\gamma_{20}\gamma_{30} & 0 & 0 \end{pmatrix} \widehat{\mathbf{u}}, \tag{2.9}$$

which has the usual zero eigenvalue associated with $\widehat{u}_3$, and two others that are real or imaginary depending on the sign of B. When $B<0$ the solutions are oscillatory with angular frequency $\gamma_{30}(-B)^{1/2}$, and it can be shown that transient growth is negligible.

2.1. *Nonlinearity*

It follows from the previous analysis that Keplerian turbulence decays in the rapid distortion limit, but that some initial conditions are subject to short-term transient growth. An interesting question is whether such growth can result in nonlinear instabilities that restart the growth cycle. We have seen above, for example, that this is the case when $\chi=0$.

In a significant numerical experiment Umurhan and Regev (2004) showed that a nonlinear two-dimensional simulation of a small Keplerian box undergoes many cycles of transient growth before eventually decaying viscously. Each of the transient episodes agreed well with the form (2.8), with the initial seed for each cycle being most probably the nonlinear evolution of some previous one.

Because vorticity is conserved in the two-dimensional inviscid limit, such flows eventually have to decay, but in three-dimensional turbulence it is at least possible that the nonlinear instabilities feed the transient growth cycle indefinitely.

Although it is impossible to predict which fluctuations would initiate nonlinear growth without actually solving the full equations, some estimates are possible. For each range of Fourier modes it is possible to define an energy and a length scale. For example, if the one-dimensional spectrum of u is $E(k)$, a reasonable velocity scale would be $u_k=(kE)^{1/2}$, and a length scale would be $L_k=2\pi/k$. One can then construct a Rossby number

$$Ro_k = \frac{u_k}{SL_k} = \frac{(kE)^{1/2}k}{2\pi S}. \tag{2.10}$$

Fluctuations for which $Ro_k\ll 1$ are dominated by the mean flow, and should behave

according to the linear theory outlined above. Fluctuations for which $Ro_k \gg 1$ decouple from the mean flow, and decay as isotropic turbulence does. Only those fluctuations for which $Ro_k = O(1)$ have any possibility of being self-sustaining.

A rough estimate of the numerical value for the threshold can be obtained by observing flows that self-sustain, even if they have a different value of χ. It is customary in shear flows to measure the Rossby number by the reduced shear $S^* = Su'^2/\epsilon$, where the dissipation rate ϵ can be written as u'^3/L_ϵ, and L_ϵ is of the order of the integral scale. It is easy to see that S^* is the inverse of a Rossby number. For typical self-sustaining shear flows, such as the near-wall region of turbulent channels, $S^* \approx 40$. The simulation by Lee *et al.* (1990) of a homogeneous inertial shear, which was tailored to approximate that case, stabilized at $S^* \approx 60$. For the simulations by Brethouwer (2005) of rotating shear at $\chi = 1$, the asymptotic value was $S^* \approx 25$, and for his case at $\chi = 3/2$, which should be close to the Keplerian case, but which decayed, it remained above $S^* = 20$. This suggests that self-sustaining fluctuations should have $Ro = O(10^{-2})$, which is encouragingly close to the observational value for α in Keplerian disks. It also emphasizes that the turbulence generated by a uniform shear, whether rotating or not, is a weak phenomenon, and that the decay of many of the simulations to date might have been caused by choosing a Rossby number that was too high.

2.2. *Viscosity*

In the same way that we have defined a Rossby number for a fluctuation with a given wavenumber, we can define a Reynolds number,

$$Re_k = \frac{u_k L_k}{\nu} = \frac{2\pi (kE)^{1/2}}{k\nu}, \tag{2.11}$$

which should be large enough for the fluctuation to survive. The evidence from self-sustaining structures in the wall region, and in highly sheared turbulence (Lee *et al.* 1990), suggests that Re_k should be at least larger than 100.

We can derive from this a rough criterion that has to be satisfied by the initial conditions for turbulence to survive. When viscosity is included in the RDT equations, the solution gets multiplied by $\exp(-\int \varepsilon k^2 \, \mathrm{d}t)$, where ε is the Ekman number defined in (1.3). Assume that the most dangerous fluctuations are those discussed in (2.8), in which $\sigma_{20} \gg 1$ and σ_{30} is small. We have seen that their inviscid amplification is approximately σ_{20} over $t \in (0,\, \sigma_{20})$. During that time $k \approx k_{10}(\sigma_{20} - t)$, and the viscous damping factor is $\exp(-\varepsilon k_{10}^2 \sigma_{20}^3/3)$. The most amplified perturbations are therefore those for which

$$\sigma_{20} \exp(-\varepsilon k_{10}^2 \sigma_{20}^3/3) \tag{2.12}$$

is maximum, which occurs for $\sigma_{20,max} = (\varepsilon k_{10}^2)^{-1/3}$. The maximum amplification is approximately $0.7\sigma_{20}$. Disregarding factors of order unity, we can then estimate the Reynolds number of those perturbations at the point of maximum amplification as

$$Re_k = \frac{2\pi \sigma_{20,max} u_0}{k_{10}\nu} \approx Re_{k,0} \varepsilon_0^{-1/3} > 100, \tag{2.13}$$

where ε_0 is based on the initial length scale L_{10}. Interpreting the initial conditions as those of the largest turbulent scales, we should only consider the fraction $\varepsilon_0^{1/3}$ of the energy that has wavenumbers near the plane $k_3 = 0$, and that lies in the sector $k_{10} \sim k/\sigma_{20,max}$. The condition (2.13) can then be manipulated into

$$Re_{L0}^{7/6} S^{*1/6} > 100, \tag{2.14}$$

which is not very restrictive, suggesting again that the limiting factor in most simulations is the choice of appropriate initial conditions, rather than the Reynolds number.

3. The numerical experiments

3.1. *Large-box computations*

The first set of numerical experiments analyzed here are two simulations chosen from a group of runs that took place over a period of one week in the Blue Gene Light computer at Lawrence Livermore National Laboratory. These runs were part of a larger set of diverse simulations that were accommodated during the final weeks of public accessibility of that computer. The runs discussed in this work used one half of the machine, with 65,536 processors.

The code uses a Fourier representation of the flowfield and is pseudospectral in the sense that aliasing errors are approximately eliminated by a sequence of eight coordinate shifts occurring over the substeps of two successive time steps. The mesh used consisted of $8192 \times 2048 \times 2048$ cells with $\Delta_1 = \Delta_2 = \Delta_3$. The number of cells in each direction, and hence the lengths of the sides of the computational box in those directions, was taken in the ratio of 4:1:1 to accommodate possible structure elongation when the shear was applied later in the run.

A preliminary run of nominally isotropic decaying turbulence was made to provide a starting field for the Keplerian shear and rotation. This isotropic run resulted in a field having a microscale Reynolds number $Re_\lambda = 216$. The peak of the energy spectrum was at approximately the eleventh numerical wavenumber, where the computational wavenumbers range from 0 to 1023. Since this field was mainly intended as an initial condition, and the dissipation was expected to decay during the spin-up, its resolution in terms of the Kolmogorov scale η is only moderate, $k_{max}\eta = 0.26$.

The nominally isotropic field was then subjected to a shear $U_1(x_2) = Sx_2$, and to rotation around the x_3-axis, intended to be at the Keplerian ratio. Unfortunately, because of a sign error, the actual parameter of the run was $\chi = -4/3$ and, while information presented below indicates that the simulations are relevant to the possibility of nonlinear instabilities in linearly-stable flows, they are not directly relevant to the Keplerian case. Two different rotation rates were chosen to give the runs different initial Rossby numbers, with values of 0.6 and 0.15 based on the one-component root-mean-squared velocity u', and on the integral scale of the turbulence. The angular velocity is handled by the code as a rotation of the frame of reference, resulting in a Coriolis force in the Navier-Stokes equations, and the shear is handled by a coordinate transformation to a grid that follows the mean shear flow. The flow is periodic in this deforming mesh. To prevent the mesh from approaching a singular state, remeshing is done periodically, as described by Rogallo (1981). The remeshings inevitably result in a loss of energy at small spatial scales but have little effect on the energetic eddies.

The evolution of the total energy is given, for both initial Rossby numbers, in figure 2(a). It decays in both cases, but it is interesting that the decay rates are different, even if the Rossby number does not appear in the linear RDT equations. This by itself suggests that nonlinearity remains important. The case with the lowest Rossby number has the slowest decay. It could perhaps be argued that the decay has virtually stopped at the end of the simulation, although the comparison in the figure reveals that this case is the closest to the results of inviscid rapid distortion theory. Sadly, it could not be continued, and it is unclear whether the slower decay is just the effect of the higher

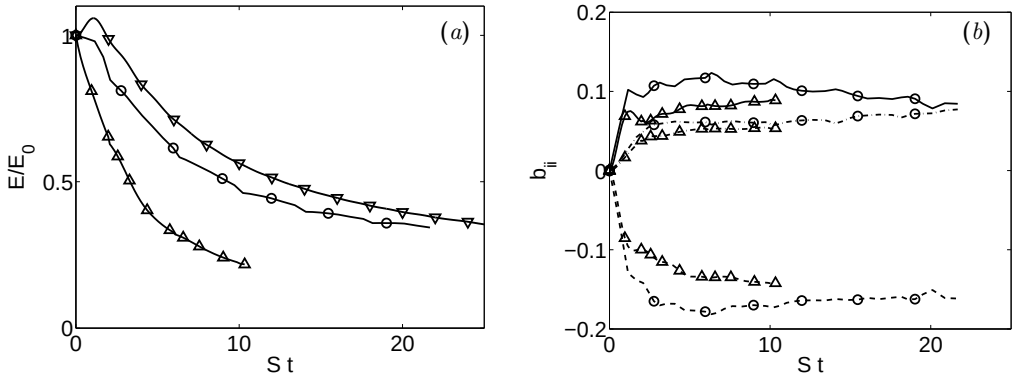

FIGURE 2. (a) Evolution of the total energy. (b) Evolution of the diagonal components of the anisotropy tensor. ——— , b_{11}; - - - - , b_{22}; —·— , b_{33}; ○ , Large-box DNS, $Ro_0 = 0.15$; △ , $Ro_0 = 0.6$; ▽ , inviscid RDT. $\chi = -4/3$.

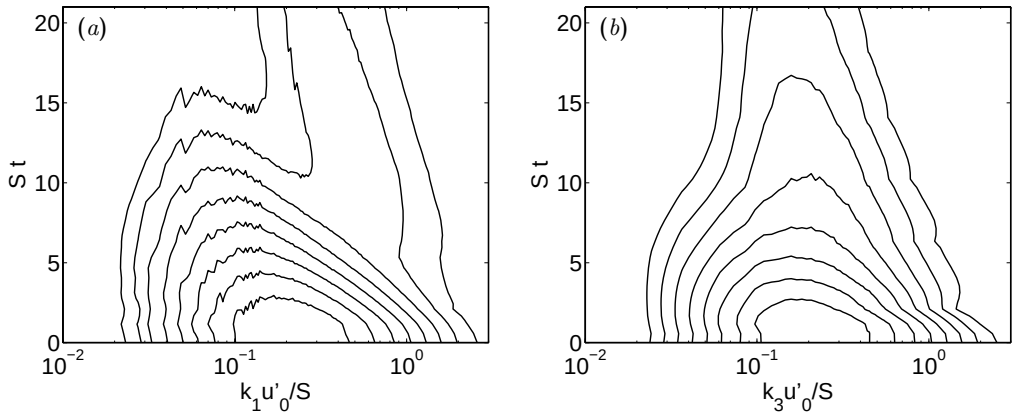

FIGURE 3. Temporal evolution of the energy spectrum with time. Each horizontal line is an instantaneous premultiplied spectrum $k_j E(k_j)$ of the total energy for, (a) the streamwise, and (b) the spanwise wavenumber. Contours are logarithmically spaced by a factor of 1.2, and the different spectra are unnormalized. Large-box DNS, $Ro_0 = 0.15$, $\chi = -4/3$.

Rossby number, or a fortuitous cancellation of viscous effects and nonlinearity. The three diagonal components of the Reynolds anisotropy tensor,

$$b_{ij} = \frac{\langle u_i' u_j' \rangle}{3u'^2} - \frac{1}{3} \tag{3.1}$$

are given in figure 2(b). They broadly follow the RDT result for this value of χ, but again both cases behave quantitatively differently.

The evolution of the energy spectra with time is given in figure 3, where each horizontal line is a premultiplied spectrum. It is clear that, although the main spectral energy peak is decaying, there is a new structure that emerges around $St = 10$, and decays much more slowly. It is centered around $(k_1, k_3) \approx (0.3, 0.15)u_0'/S$, where u_0' is the r.m.s. velocity at the beginning of the spin-up. This peak has no counterpart in linear theory, because the inviscid RDT equations (2.4) do not contain k explicitly, and are only sensitive to the direction of the wave vector. They cannot therefore generate preferred length scales, that have to come from either viscous or nonlinear effects, or from the initial conditions. In

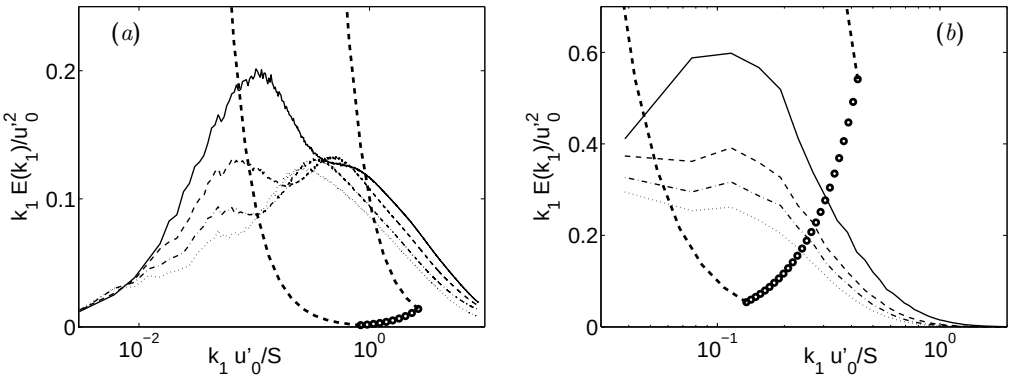

FIGURE 4. Premultiplied spectra of the kinetic energy for, (*a*) Large-box simulation, $\chi = -4/3$, $Ro_0 = 0.15$. ——— , $t = 7.6$; - - - - , $t = 12$; —·— , $t = 16.8$, ····· , $t = 21.7$. (*b*) Small-box simulation, $\chi = 4/3$. ——— , $t = 2.96$; - - - - , $t = 4.97$; —·— , $t = 5.98$; ····· , $t = 6.98$. In both cases, the thick dashed lines bound the region $Ro_k \in (0.005, 0.05)$, and the circles mark $Re_k = 100$, as defined in (2.10).

Integral scale, $L = (3\pi/4), (\int k^{-1}E(k)dk / \int E(k)dk)$	0.35
Rossby number, $Ro = u'_0/SL$	0.11
Ekman number, $\varepsilon = \nu/SL^2$	0.001
Kolmogorov resolution, $k_{\max}\eta$	1.82
Re_λ	46
Reduced shear, S^*	15.2

TABLE 1. Turbulence characteristics of the initial velocity field in the small-box simulation.

the present case, the secondary peak is too far from the dissipative scales for viscosity to play a role, and the scale disparity in figure 3(*a*) makes it unlikely that the peak derives from the initial conditions.

As such, this peak is an obvious candidate for a nonlinearly growing feature that may eventually result in self-sustained turbulence. In fact, when the spectra are plotted individually, as in figure 4, the surviving peak turns out to be near $Ro_k = 0.01$, in agreement with the estimations of section 2.1.

3.2. *Small-box computations*

A second set of numerical experiments was carried out during the summer program to probe the stability of the Keplerian case, $\chi = 4/3$, and includes both direct simulations and inviscid RDT runs. The former use essentially the same pseudospectral code described in the previous section, but on a considerably smaller grid, due to time and computational constraints. The RDT runs were carried out using the Particle Representation Model of Kassinos and Reynolds (1996).

All the DNS runs presented here have a resolution of 256^3 Fourier modes in a $(2\pi)^3$ computational domain. The initial conditions for the velocity were common to all cases. They were created starting with a pulse of energy at low wave numbers, and a random distribution of phases for the Fourier modes. In order to let the higher-order statistics

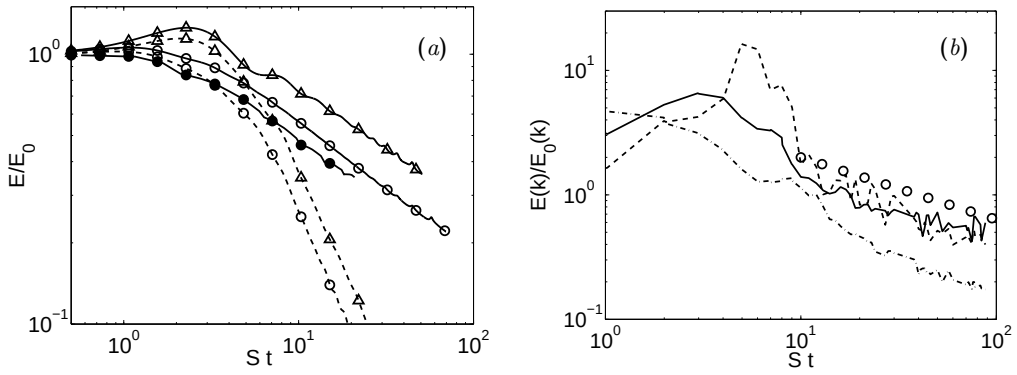

FIGURE 5. (a) Evolution of the total turbulent kinetic energy, normalized by its initial value. Solid lines are DNS, dashed ones are RDT. ∘ , small-box $\chi = -4/3$; • , large-box $\chi = -4/3$, $Ro = 0.15$; △ , small-box $\chi = 4/3$. (b) Energy in individual wavenumber shells, normalized by their initial values, for the small-box Keplerian DNS. - - - - , $k = 1\,(ku_0'/S = 0.04)$; ——— , $k \in (2,\,3)\,(ku_0'/S = 0.075 - 0.11)$; —·— , $k \in (4,\,7)\,(ku_0'/S = 0.15 - 0.27)$; ∘ , $E \sim t^{-1/2}$.

develop, the flow evolved in the absence of either mean shear or frame rotation, while forcing was applied to the low-wavenumber region of the spectrum. This initial phase was continued until an equilibrium state was reached, and the skewness acquired its peak value. At that time, hereafter referred to as $t = 0$, the mean shear and frame rotation were switched on, while the artificial forcing was eliminated. The characteristics of the initial field are summarized in table 1.

The evolution of the turbulent kinetic energy, normalized by its value at the instant at which the mean shear is applied, is shown in figure 5(a). The evolution histories obtained from the DNS are shown as solid lines, while those obtained from RDT are shown dashed. In both cases the long-term evolution histories for $\chi = -4/3$ and $\chi = 4/3$ are similar, with a power-law exponent which is close to $-1/2$ for the RDT. Initially the Keplerian case has a strong transient growth which is much weaker for the case $\chi = -4/3$. This initial phase is also found in the DNSes, although the small-box simulations decay much faster after $St \approx 5$, presumably because viscosity becomes dominant. The large-box simulation does not enter the viscous phase, and follows fairly closely the inviscid RDT. As was the case in the discussion of figure 2, it is unclear whether the decay rate might slow slightly at the end of that simulation.

The evolution of the one-dimensional energy spectra in the Keplerian case is shown in figure 4(b), which should be contrasted to figure 4(a). While the emergence of a second persistent peak is not as pronounced as in the $\chi = -4/3$ large-box case, there is a hint of a second peak developing after about $St = 5$, while the energy decay seems at that point to collapse into a more or less universal rate, which is very close to a power law with exponent $-1/2$. In this case, the second peak is also within the correct range of Rossby numbers, while the main difference with figure 4(a) is the unavoidably much lower Reynolds numbers of the fluctuations.

Another way to probe for a possible range of scales where the turbulent kinetic energy equilibrates is to plot the total energy per spherical shell in Fourier space. This is done for the small-box Keplerian case in figure 5(b), which covers approximately the same wavenumber range as the second energy peak in figure 4(b), but which extends for a longer time interval. It is remarkable that the energy in the first two wavenumber shells undergoes initially a fairly large transient growth, of the order of 20 for the first one.

It is even more interesting that both shells appear to equilibrate at long times, even at these low Reynolds numbers. In particular, the second shell, which corresponds to the central part of the range of critical Rossby numbers in figure4(b), seems to be almost at equilibrium at the end of the simulation. Shells with wavenumbers much higher than those represented in the figure decay viscously for most of the simulation interval.

4. Discussion

We have presented simulations of rotating sheared turbulence for both the Keplerian case, $\chi = 4/3$, and for $\chi = -4/3$. Both cases are linearly stable, and all the simulations decay, but there is a strong effect of the Reynolds number that is clearly visible in the different long-term behaviors of the simulations in large and small computational grids. While the latter enter an apparently viscous regime for $St = O(1)$, the former track the inviscid RDT solutions for much longer times.

The RDT solutions in both cases decay with a similar power-law exponent, $-1/2$, but the Keplerian case undergoes an appreciable initial transient growth, that is absent when $\chi = -4/3$. Unfortunately is was only possible to run the latter case in a large computational grid, in spite of which there are indications of nonlinear growth in a range of wavenumbers that could conceivably lead to self-sustaining turbulence in protoplanetary accretion disks. This secondary peak is present for both shear ratios, and is associated in both cases with eddy Rossby numbers of the order of 10^{-2}, and with eddy Reynolds numbers larger than a few hundred. Although additional simulations are needed, these observations suggest the range of parameters in which self-sustaining Keplerian turbulence might be found, and emphasize the importance of simulations with resolutions and Reynolds numbers higher than those that have been used up to now in the study this problem.

Acknowledgments

This work was supported in part by the ASC program of the DoE, and by grant TRA2006-08226 of the Spanish CICYT.

REFERENCES

Akylas, E., Kassinos, S. C. and Langer, C. A. 2006 An analytical solution for rapidly distorted turbulent shear flow in a rotating frame. *Phys. Fluids* **18**, 085104.

Balbus, S. A. 2003 Enhanced angular momentum transport in accretion disks. *Ann. Rev. Astron. Astroph.* **41**, 555–597.

Balbus, S. A., Hawley, J. F. and Stone, J. M. 1996 Nonlinear stability, hydrodynamic turbulence and transport in disks. *Astroph. J.* **467**, 76–86.

Bardina, J. 1983 Improved turbulence models based on large eddy simulation of homogeneous, incompressible, turbulence flows. PhD thesis, Stanford University.

Beckwith, S. V. W. and Sargent, A. E. 1993 The occurence and properties of disks around young stars. In *Protostars and protoplanets III* (ed. E. H. Levy and J. I. Lunine), pp. 521–541. U. Arizona Press, Tucson.

Bradshaw, P. 1969 The analogy between streamline curvature and buoyancy in turbulent shear flow. *J. Fluid Mech.* **36**, 177–191.

Brethouwer, G. 2005 The effect of rotation on radidly sheared homogeneous turbulence and passive scalar transport. Linear theory and direct numerical simulation. *J. Fluid Mech.* **542**, 305–342.

Calvet, N., Lee, H. and Strom, S. E. 2000 Evolution of disk accretion. In *Protostars and protoplanets IV* (ed. V. Mannings, A. P. Boss and S. S. Russell), pp. 377–399. U. Arizona Press, Tucson.

Cambon, C. and Scott, J. F. 1999 Linear and nonlinear models of anisotropic turbulence. *Ann. Rev. Fluid. Mech.* **31**, 1–53.

Dubrulle, B. 1993 Differential rotation as a source of angular momentum transfer in the solar nebula. *Icarus* **106**, 59–76.

Dubrulle, B., Marie, L., Normand, C., Richard, D., Hersant, F. and Zahn, J. P. 2005 A hydrodynamic shear instability in stratified disks. *Astron. Astrophys.* **429**, 1–13.

Dubrulle, B. and Zahn, J. P. 1991 Nonlinear instability of viscous couette flow. part 1. analytical approach to a necessary condition. *J. Fluid Mech.* **231**, 561–573.

Kassinos, S. C. and Reynolds, W. C. 1996 A particle representation model for the deformation of homogeneous turbulence. In *Ann. Res. Briefs*, pp. 31–50. Center Turb. Res., Stanford.

Lee, M. J., Kim, J. and Moin, P. 1990 Structure of turbulence at high shear rates. *J. Fluid Mech.* **216**, 561–583.

Lin, D. N. C. and Papaloizou, J. C. B. 1996 Theory of accretion disks II: Application to observed systems. *Ann. Rev. Astron. Astroph.* **34**, 703–748.

Lynden-Bell, D. and Pringle, J. E. 1974 The evolution of viscous discs and the origin of the nebular variables. *Mon. Not. Roy. Astron. Soc.* **168**, 603–637.

Papaloizou, J. C. B. and Lin, D. N. C. 1995 Theory of accretion disks I: Angular momentum transport processes. *Ann. Rev. Astron. Astroph.* **33**, 505–540.

Pedley, T. J. 1969 On the stability of viscous flows in a rapidly rotating pipe. *J. Fluid Mech.* **35**, 97–115.

Pierrehumbert, R. T. 1986 Universal short-wave instability of two-dimensional eddies in an inviscid fluid. *Phys. Rev. Lett.* **57**, 2157–2159.

Pringle, J. E. 1981 Accretion discs in astrophysics. *Ann. Rev. Astron. Astroph.* **19**, 137–162.

Rayleigh, L. 1917 On the dynamics of revolving fluids. *Proc. Roy. Soc. London* A **93**, 148–154, (*Scientific papers*, **6**, 447–453. Cambridge Univ. Press).

Rogallo, R. 1981 Numerical experiments in homogeneous turbulence. Tech. Memo 81315. NASA.

Rogers, M. M. and Moin, P. 1987 The structure of the vorticity field in homogeneous turbulent flows. *J. Fluid Mech.* **176**, 33–66.

Salhi, A. and Cambon, C. 1997 An analysis of rotating shear flow using linear theory and dns and les results. *J. Fluid Mech.* **347**, 171–195.

Schmid, P. and Henningson, D. 2001 *Stability and transition in shear flows*. Springer.

Shakura, N. I. and Sunyaev, R. A. 1973 Black holes in binary systems. observational appearance. *Astron. Astrophys.* **24**, 337–355.

Stone, J. M., Gammie, C. F., Balbus, S. A. and Hawley, J. F. 2000 transport processes in protostellar disks. In *Protostars and protoplanets IV* (ed. V. Mannings, A. P. Boss and S. S. Russell), pp. 589–611. U. Arizona Press, Tucson.

Tavoularis, S. and Karnik, U. 1989 Further experiments on the evolution of turbulent stresses in uniformly sheared turbulence. *J. Fluid Mech.* **204**, 457–478.

Umurhan, O. M. and Regev, O. 2004 Hydrodynamic stability of rotationally supported flows: linear and nonlinear 2D shearing box results. *Astron. Astrophys.* **427**, 855–872.